A synthetic Earth gravity model designed specifically for testing regional gravimetric geoid determination algorithms

I. Baran
Western Australian Centre for Geodesy, Curtin University of Technology, GPO Box U1987, Perth, WA 6845, Australia, Tel: +61 8 9266 2582; Fax: +61 8 9266 2703; E-mail: barani@vesta.curtin.edu.au

M. Kuhn (corresponding author)
Western Australian Centre for Geodesy, Curtin University of Technology, GPO Box U1987, Perth, WA 6845, Australia, Tel: +61 8 9266 7603; Fax: +61 8 9266 2703; E-mail: M.Kuhn@curtin.edu.au

S.J. Claessens
Western Australian Centre for Geodesy, Curtin University of Technology, GPO Box U1987, Perth, WA 6845, Australia, Tel: +61 8 9266 2218; Fax: +61 8 9266 2703; E-mail: claesses@vesta.curtin.edu.au

W.E. Featherstone
Western Australian Centre for Geodesy, Curtin University of Technology, GPO Box U1987, Perth, WA 6845, Australia, Tel: +61 8 9266 2734; Fax: +61 8 9266 2703; E-mail: W.Featherstone@curtin.edu.au

S.A. Holmes
Raytheon ITSS, 1616 McCormick Drive, Upper Marlboro, Maryland, 20774, USA
Tel.: +1-301-883-4036; Fax: +1-301-794-4140; Email: simon_a_holmes@raytheon.com

P. Vaníček
Department of Geodesy and Geomatics Engineering, University of New Brunswick, PO Box 4400, Fredericton, E3B 5A3, Canada, Tel: +1 506 453 5144; Fax: +1 506 453 4943; E-mail: vanicek@unb.ca

Abstract - A Synthetic [simulated] Earth Gravity Model (SEGM) of the geoid, gravity and topography has been constructed over Australia specifically for validating regional gravimetric geoid determination theories, techniques and computer software. This regional high-resolution (1-arc-min by 1-arc-min) Australian SEGM (AusSEGM) is a combined source and effect model. The long-wavelength effect part (up to and including spherical harmonic degree and order 360) is taken from an assumed errorless EGM96 global geopotential model. Using forward modelling via numerical Newtonian integration, the short-wavelength source part is computed from a high-resolution (3-arc-sec by 3-arc-sec) synthetic digital elevation model (SDEM), which is a fractal surface based on the GLOBE v1 DEM. All topographic masses are modelled with a constant mass-density of 2670 kg/m^3. Based on these input data, gravity values on the synthetic topography (on a grid and at arbitrarily distributed discrete points) and consistent geoidal heights at regular 1-arc-min geographical grid nodes have been computed. The precision of the synthetic gravity and geoid data (after a first iteration) is estimated to be better than 30 μGal and 3 mm, respectively, which reduces to 1 μGal and 1 mm after a second iteration. The second iteration accounts for the changes in the geoid due to the superposed synthetic topographic mass distribution. The first iteration of AusSEGM is compared with Australian gravity and GPS-levelling data to verify that it gives a realistic representation of the Earth's gravity field. As a by-product of this comparison, AusSEGM gives further evidence of the north-south-trending error in the Australian Height Datum. The freely available AusSEGM-derived gravity and SDEM data, included as Electronic Supplementary Material (ESM) with this paper, can be used to compute a geoid model that, if correct, will agree exactly with the AusSEGM geoidal heights, thus offering independent verification of theories and numerical techniques used for regional geoid modelling.

Keywords: Synthetic Earth gravity model (SEGM), gravity, regional geoid determination, topography, Newtonian integration, forward modelling, Australia

1. Introduction

In 1996, the International Association of Geodesy (IAG) created the special study group SSG3.177 "*Synthetic modelling of the Earth's gravity field*" (http://www.cage.curtin.edu.au/~will/iagssg3177.html) with the primary objective of constructing synthetic Earth gravity models (SEGMs) to be used in geodesy. Such models were previously unavailable to the geodetic community, which is at odds with other Earth sciences, notably seismology with the Preliminary Reference Earth Model (PREM; Dziewonski and Anderson 1981). Instead, geodetic gravity field modelling often tends to rely on empirical methods to validate results (and thus implicitly the theories and software). A notable example is comparisons of regional gravimetric geoid models with GPS-levelling data on land, where the GPS-levelling control data contain a variety of generally poorly known errors. A global or regional SEGM avoids this problem and is thus a useful tool for an independent and more objective validation of gravity field determination and modelling methods. In addition, other working groups of the IAG commission "*Gravity Field*" (http://www.ceegs.ohio-state.edu/iag-commission2/index.html) rely on the availability of an SEGM.

In the framework of IAG SSG3.177, several authors have constructed different SEGMs, as well as others constructed independently of this SSG or before its creation (see the citations in the review by Featherstone (1999)). However, none of these previous SEGMs have specifically addressed the issue of practical regional geoid computations in the presence of topography. Instead, they only generate the external gravity field, either outside the topography (e.g., Pail 2000, Haagmans 2000, Claessens 2003, Kuhn and

Featherstone 2005), or implicitly assuming that it had been properly condensed onto or moved below the synthetic geoid (e.g., Tziavos 1996, Featherstone and Olliver 1997, Featherstone 2002b, Novák et al. 2001). However, it is the presence of topography that makes the task of local geoid determination difficult.

Acknowledging the work of Ågren (2004), the SEGM presented in this paper aims to remedy this deficiency by including a synthetic topography with a constant mass-density (in the first version), inside which the synthetic geoid is known and is consistent with synthetic gravity values on the synthetic topography. Importantly, all these synthetic surfaces and values are designed to be as realistic as possible, which will be verified later in this paper with observational data. The resulting SEGM is provided in terms of the data types that are routinely used in regional geoid determination (i.e., discrete gravity values on the Earth's surface, their coordinates, a spherical harmonic global geopotential model (GGM) and a regular digital elevation model (DEM)).

The SEGM can then be used to resolve some of the differences currently encountered among those who compute geoid models around the world (e.g., Vaníček and Kleusberg 1987, Véronneau et al. 2000, Featherstone et al. 2001, Nahavandchi and Sjöberg 2001, Smith and Roman 2001, Kuroishi et al. 2002, among many others). However, only a few comparisons of different geoid computation techniques using the same input data have yet been presented (e.g., Tziavos 1996, Featherstone et al. 2004, Ellman, in press). This situation can be significantly improved with the SEGM presented here. Most importantly, any SEGM must rely upon as few assumptions as possible so that it can reliably be used to test practical geoid determination with a view to the current goal of the 1 cm geoid. In addition, the use of widely accepted models of the Earth's shape and gravity field should guarantee that the results from the SEGM are applicable to real Earth situations.

2. Concepts of Synthetic Earth Gravity Models

There are two main approaches to synthetic gravity field modelling: *source models*, which take into account the mass-density distribution inside the solid Earth by forward modelling via Newton's integral (e.g., Pail 2000, Kuhn and Featherstone 2005); and *effect models*, which do not make any assumptions about the mass-density distribution inside the Earth, but use information of the observed gravity field (e.g., Tziavos 1996, Novák et al. 2001, Featherstone 2002b). The SEGM described here uses a self-consistent combination of both approaches for the reasons of computational convenience and also to ensure that it is realistic.

Existing Earth models derived from observed data, namely the EGM96 global geopotential model (Lemoine et al. 1998), the GLOBE v1 global DEM (Hastings and Dunbar 1998) and the JGP95E global DEM (Lemoine et al. 1998 chap 2), have been used to provide the global gravity field and topography, since these models are freely available. GLOBE was used in preference to JGP95E over Australia because of a discontinuity in JGP95E at 160°E due to the use of two different data sources (Hilton et al. 2003), and JGP95E was used elsewhere. Using existing Earth models ensures that the broad structure of the SEGM is realistic, but it also saves computational time. These models provide the long-wavelength geoid and gravity component of the SEGM and are considered as error-free. Importantly, this assumption is permitted for a synthetic model.

The high-resolution, regional SEGM over the continent of Australia, herein termed AusSEGM, is constructed through the superposition of high-resolution simulated local data onto the aforementioned global models. Specifically, the high-frequency topographic effects on gravitational attraction and potential (and the corresponding geoidal height after using Bruns's formula) are generated via Newton's integration (i.e., forward modelling) that uses both local and global topographic masses. The final gravity and geoid data from

AusSEGM are obtained by adding together the long- and short-wavelength parts (Fig. 1). As such, regional geoid computations using AusSEGM can only be tested over the Australian region. However, the methods described here can readily and easily be applied to other regions.

Figure 1 near here

3. Construction of the synthetic DEM (SDEM)

The 9-arc-sec by 9-arc-sec version 2 DEM (DEM-9S) of Australia (Hutchinson 2001; http://www.ga.gov.au/nmd/products/digidat/dem_9s.htm) was not in the public domain when the construction of AusSEGM began. Therefore, a high-resolution (3-arc-sec by 3-arc-sec) DEM was simulated over Australia using a fractal surface based on the (30-arc-sec by 30-arc-sec) "GLOBE v1" global DEM (Section 3.1). Any other approach or data source could be used to construct the synthetic DEM (SDEM), but it should be as realistic as possible. Also, any arbitrarily fine resolution SDEM can be simulated, but for the reasons of data management, computational speed and the accuracy attainable from forward modelling (Kuhn and Featherstone 2005), a 3-arc-sec SDEM was simulated. The (5-arc-min by 5-arc-min) JGP95E global DEM was used to model the topographic masses outside of Australia using the approach of equivalent rock heights (cf. Rummel et al. 1988).

Within the philosophy of an SEGM, the adopted SDEM is considered to represent a realistically simulated Earth's surface. Therefore, the heights of all points located on this simulated Earth's surface are given by the values of the SDEM. Also, the topographic heights of all these DEMs are assumed to be orthometric heights referred to the EGM96

spheroid (up to degree and order 360). However, some subtleties arise from this assumption, which will be discussed in Section 6.

3.1 The high-resolution SDEM for AusSEGM

The 3-arc-sec by 3-arc-sec (~100m) SDEM over Australia (112°E-155°E, 8°S-45°S) was constructed by combining two complementary components: (i) a 3-arc-sec DEM obtained by bi-linear interpolation from the 30-arc-sec GLOBE v1 global DEM; and (ii) an isotropic 2D fractal surface defined at the same 3-arc-sec resolution. The lateral variability of the fractal surface was associated with the roughness of GLOBE, which ensures a reasonably realistic fractal contribution to the final SDEM (described below).

Both components together ensure that the broad structure of the SDEM is similar to the GLOBE and that it contains (simulated) topographical information up to the 3-arc-sec by 3-arc-sec resolution. Over marine areas (as defined by the GLOBE DEM), the SDEM height was set to zero. To distinguish between land and ocean areas for later analysis, a land-ocean function was derived for the same area (the value "0" over ocean areas and "1" over land). This information is necessary because some parts of the Australian continent are below mean sea level (e.g., Lake Eyre, $\lambda \approx 137°E$, $\varphi \approx 28°S$), so the heights here should not be set to zero as over ocean areas.

A summary of all tasks involved in constructing the SDEM is given below:

- The GLOBE DEM between (112°E-155°E, 8°S-45°S) was divided into rectangular cells with dimensions 5-arc-min by 5-arc-min, each with an overlap of 2.5-arc-min. Each cell was re-sampled from 30-arc-sec to 3-arc-sec resolution using bi-linear interpolation. For all cells that include land elevation data (i.e., land-ocean function = 1), a plane was fitted to all the DEM heights and subtracted in order to derive a

standard deviation (SD) that is free from any linear trends. Subsequently, the SD was taken as a measure of the spatial and vertical terrain variation (ruggedness).

- The fractal surface with a power-law behaviour of each interpolated cell (including overlap) was computed according to Adler (1981). Here the power-law exponent (b) of the fractal surface is related to the SD and computed according to:

$$b = \frac{1.5}{1.001^{(8 \cdot SD)}} \tag{1}$$

The parameter b controls the horizontal variation of the fractal surface; if b is small, the variation is large, and vice versa. Furthermore, Eq. (1) ensures that for $b = 1.5$, a prescribed minimum value of $SD = 1$ m, is obtained. A small value of b (large SD) results in a fractal surface of a predominantly short-wavelength structure (i.e., suitable for rugged mountainous areas), whereas a large value of b (small SD) produces a fractal surface of a mostly long-wavelength character (i.e., suitable for plain/plateau areas). After the fractal surface was computed for each cell of the interpolated DEM, it was point-wise multiplied by the land-ocean function in order to only extract values over land.

- The magnitude of the fractal surface (MF) was established according to:

$$MF = F \cdot SD \cdot scale \tag{2}$$

where $scale$ was set to 0.30, which means that MF represents 30% of the standard deviation of GLOBE. The parameter F stands for the unit magnitude of the fractal surface (i.e., a random value between zero and one). The 30% relationship was chosen empirically, by trial and error, such that the fractal surface gives a realistic representation of the local topography.

- A 2D trapezoidal filter was applied to adjacent cells in order to ensure that no artificial steps were introduced. This filter was designed so that the overlap area of one cell is multiplied with a factor that decreases linearly from one at the edge of

the cell to zero at the edge of the overlap area, and the same overlap area from the adjacent cell is multiplied with a factor increasing linearly from zero to one.

- To obtain the final SDEM, the values of the fractal surface were added to the 3-arc-sec DEM obtained by bi-linear interpolation from GLOBE.

Importantly, the parameters and relationships used in Eqs. (1) and (2) were chosen so as to provide a realistic SDEM. The numerical values of these parameters could, of course, be chosen in a different way, provided that the resulting SDEM and SEGM are sufficiently close to reality.

Figure 2 shows a generalised image of 3-arc-sec by 3-arc-sec SDEM over Australia, from which the broad structure of the Australian topography, as defined by GLOBE v1, is evident. In order to prove that this SDEM is realistic, it was compared with DEM-9S v2 over Australia, where the SDEM was arithmetically averaged to a 9-arc-sec resolution. The comparison (Fig. 3) shows that the broad structure of the SDEM is realistic, as most (91.4%) of the differences are <100 m. Moreover, the differences agree with those found by Hilton et al. (2003, Fig 2d), which indicates that they are mainly due to errors in the source data used in GLOBE v1 rather than in the fractal surface.

Figures 2 and 3 near here

Naturally, it would be more realistic to use a re-sampled DEM-9S v2 Australian DEM together with a fractal surface. However, we did not do this because (i) this DEM was not in the public domain at that time (it is now available at http://www.ga.gov.au/nmd/products/digidat/dem_9s.htm) and so we could not supply it to a potentially wide variety of 'users', and (ii) we wanted to devise and present a method that could easily and transparently be applied by others to generate their own SEGM. Since a

SDEM is an essential ingredient in a SEGM, it is important to be able to provide both data sets to ‘users’.

3.2 The global DEM for AusSEGM

The global topography (assumed relative to EGM96; see Section 6) was modelled by the (5-arc-min by 5-arc-min) JGP95E global DEM, which was developed as one component of the EGM96 (Lemoine et al. 1998, Chapter 2) and released entirely in 1996 (ftp://cddisa.gsfc.nasa.gov/pub/egm96/gravity_data/topo.jgp95e.min05.Z). As such, it is more consistent with EGM96 than, say, GLOBE v1. Also, JGP95E classifies the terrain into six different types (1: dry land below mean sea level (MSL), 2: lake, 3: oceanic ice shelf, 4: ocean, 5: glacier ice, 6: dry land above MSL). These different mass distributions were converted into equivalent rock heights (using mass balance formulae given in spherical approximation of the height reference surface; Rummel et al. 1988) with respect to the constant topographic mass-density of 2670 kg/m^3 (cf. Kuhn and Seitz 2005), which then serves as the global SDEM with a 5-arc-min by 5-arc-min resolution. Furthermore, the area over Australia (112°E-155°E, 8°S-45°S) was replaced by the (3-arc-sec) SDEM (arithmetically averaged to a 5-arc-min resolution), which ensures that there is no difference in mass caused by the use of different DEMs with different resolutions.

4. Methodology used to construct AusSEGM

AusSEGM is a combined source- and effect-SEGM that is composed of two parts representing its long- and short-wavelength components. The long-wavelength part (in terms of gravity and geoidal height) is taken directly from EGM96 (cf. Tziavos 1996; Featherstone 2002b). The short-wavelength part is derived from the local and global topographic information using forward modelling by numerical Newtonian integration

using spherical tesseroids (spherical volume elements) approximated by prisms of equal mass and height (e.g., Kuhn 2003). As all input data are assumed to be error-free, an exact (spectral) separation into long- and short-wavelength parts can be performed without having the problem that the errors present in these data sets cannot be easily split into their spectral constituents, as is often the case with real measurements (e.g., errors in JGP95E propagate into the EGM96).

Here the spectral separation was implemented at the maximum degree and order of EGM96 (N_{max}=360), since this value is very commonly used in regional geoid determinations. As such, it is important for an SEGM to provide data in a form that is adopted by a wide range of 'users'. We admit that this choice is somewhat arbitrary for AusSEGM because it has no reference to any geological knowledge of the Australian continent. However, as will be shown in Section 5, the power spectrum from AusSEGM seamlessly interfaces with that of EGM96, so the spectral separation at N_{max}=360 is justified.

4.1 Generation of the long-wavelength part of AusSEGM

As stated, the long-wavelength geoid and gravity parts of AusSEGM are taken from EGM96 to ensure that the general structure of AusSEGM is realistic. Two parameters were extracted from EGM96, namely (i) free-air gravity anomalies at the Earth's surface $\Delta g_{GGM}^{N_{\max}}(\Omega, H)$, and (ii) geoidal heights $N_{GGM}^{N_{\max}}(\Omega)$ using the spherical harmonic synthesis formulae as given by Lemoine et al. (1998, Eqs 11.4-2 and 5.21-29). Here, Ω stands for the geographical coordinate pair (λ: longitude, φ: latitude) and H indicates the orthometric height, which is given by the SDEM and referred (in the first iteration; see Section 6) to EGM96. In the following, all parameters with the superscript N_{max}, indicate that they contain only spectral information up to and including degree and order $N_{max} = 360$.

The free-air gravity anomalies $\Delta g_{GGM}^{N_{\max}}(\Omega,H)$ have been converted into gravity values at the simulated Earth's surface (SDEM) by adding normal gravity $\gamma(\Omega,H)$, computed from Somigliana's formula with the GRS80 parameters (Moritz 1980) at the same location (Ω,H) with H as given by the SEDM, which results in (i.e., the gravity anomalies were not upward-continued from the telluroid to the Earth's surface)

$$g_{GGM}^{N_{\max}}(\Omega,H) = \Delta g_{GGM}^{N_{\max}}(\Omega,H) + \gamma(\Omega,H) \tag{3}$$

Importantly, normal gravity was computed with the same formula as used for the data preparation for EGM96 (Lemoine et al. 1998, p. 3-13). Also, the spherical harmonic synthesis can be used to generate both randomly distributed and gridded values.

4.2 Generation of the short-wavelength part of AusSEGM

The short-wavelength part of gravity at the simulated Earth's surface and short-wavelength geoidal undulations for AusSEGM were modelled by the effect of local and global topographic masses on gravitational attraction and potential, respectively. These effects have been determined by numerical Newton integration using the constant density of 2670 kg/m^3 for the topographical masses (cf. Kuhn and Featherstone 2005). This was necessary because neither a 2D nor a 3D digital density model of the Australian topography exists yet. The local topographical masses are based on the 3-arc-sec by 3-arc-sec SDEM (Section 3.1), and the global topographical masses (outside the area 112°E-155°E, 8°S-45°S) are based on the equivalent rock heights of the 5-arc-min by 5-arc-min JGP95E global DEM, as explained earlier. In terms of gravity field modelling, the equivalent rock heights will correctly account for all distant mass-density anomalies.

It should be mentioned that, in principle, it is not necessary to estimate the effect (on both gravity and potential) of the global topographical masses, as the effect of more distant masses has a very smooth behaviour (spectral content mostly below N_{max} = 360),

and is thus already contained in the global geopotential model. Moreover, these effects have to be removed because they are already included in the long-wavelength part (described later). In other words, the N_{max} = 360 component of JGP95E is included in EGM96, so it should not be added again from the global forward modelling for the SEGM.

However, it is not possible to define a constant radius (a spherical cap) around the computation point for the Newtonian integration that *exactly* extracts the spectral content up to degree N_{max} of the effect on gravitational attraction and potential. This is because of the imperfect high-pass filtering properties of a spherical cap (cf. Vaníček and Featherstone 1998). To avoid this problem, the gravitational effect of the complete global topographic masses is considered here, and subsequently separated into its long- and short-wavelength parts by a surface spherical harmonic analysis. As such, only the short-wavelength part is considered in the sequel.

In order to further save computation time, the DEMs have been generalised (by arithmetical averaging) to coarser resolutions for more distant masses (with respect to each computation point), as shown in Table 1. This computation follows the concepts outlined in, e.g., Kuhn (2003). It is based on numerical integration using the effects of spherical tesseroids approximated by prisms of equal mass and height.

Table 1 near here

For the computation of the short-wavelength part of gravity at the simulated Earth's surface and geoidal undulations at each point, the 3-arc-sec resolution SDEM is used for the topographic masses in the near vicinity of the computation point, and coarser resolutions are used for more distant masses. The computation areas are bounded by meridians and parallels (i.e., spherical rectangles). These areas are defined by their

extensions in longitude λ_r, and latitude φ_r for DEMs of finer resolution and by fixed areas for DEMs of coarser resolutions (Table 1). Importantly, the extensions (λ_r, φ_r) - and thus the computation areas - were chosen empirically in such a way that the corresponding approximation error (with respect to the finer resolution) always remains below 0.01 m^2s^{-2} for the potential (~1 mm in geoidal height) and 1 μGal for the gravitational attraction.

The gravitational acceleration effects at the simulated Earth's surface $\delta g_{SDEM}(\Omega, H)$ and at the geoid $\delta g_{SDEM}(\Omega, H=0) = \delta g_{0,SDEM}(\Omega)$ caused by all (local and global) topographic masses are illustrated in Figs. 4 and 5. The spatial structure of both effects is very similar; only the magnitude changes from positive values in Fig. 4 to generally negative values in Fig. 5. The negative values for $\delta g_{0,SDEM}(\Omega)$ are due to the fact that the topographic masses in the near vicinity of the computation point are located above the computation point (except near Lake Eyre, λ≈137°E, φ≈28°S), thus their gravitational attraction acts away from the geocentre to lower the gravity value on the geoid. Overall, a high correlation with the SDEM can be seen (cf. Figs. 4 and 5 with Fig. 2).

Figures 4 and 5 near here

The effect on the gravitational potential at the geoid $\delta V_{SDEM}(\Omega, H=0) = \delta V_{0,SDEM}(\Omega)$ caused by all (local and global) topographic masses (Fig. 6) is much smoother (potential is a smoother function than gravitational attraction; e.g., Heiskanen and Moritz 1967). Only a long-wavelength correlation with topography can be seen in Fig. 6, which is predominantly due to the inclusion of the global topography. This feature occurs because the inverse-distance function for the gravitational potential used in the Newtonian integration puts relatively more weight on the effect of

distant masses than that of the gravitational attraction (i.e., inverse distance versus inverse distance-squared). This gravitational potential term was converted into the effect on the geoidal height using Bruns's formula (e.g., Heiskanen and Moritz 1967, p. 85)

$$\delta N_{SDEM}(\Omega) = \frac{\delta V_{0,SDEM}(\Omega)}{\gamma_{ell}(\Omega)} \tag{4}$$

where $\gamma_{ell}(\Omega)$ is normal gravity on the surface of the GRS80 reference ellipsoid. Obviously, the topographical effect on the geoidal height $\delta N_{SDEM}(\Omega)$ has almost the same structure as $\delta V_{0,SDEM}(\Omega)$ shown in Fig. 6, except the amplitudes are approximately one order of magnitude smaller.

Figure 6 near here

Bruns's formula (Eq. 4) only represents the linear part of a series expansion (e.g., Heiskanen and Moritz 1967). However, it is accurate to better than $1.5 \times 10^{-7}(\mathrm{m}^{-1})\ N^2$ (Vaníček and Martinec 1994), which is equivalent to a maximum error of 1.5 mm for a maximum geoidal height of 100 m. Therefore, the maximum error over Australia remains below 1 mm, as the maximum Australian geoidal height is about 70 m (Featherstone et al. 2001), which is better than our desired 1 mm accuracy for the AusSEGM.

As mentioned earlier, the parameters $\delta g_{SDEM}(\Omega, H)$, $\delta g_{0,SDEM}(\Omega)$, $\delta V_{0,SDEM}(\Omega)$ and $\delta N_{SDEM}(\Omega)$ are derived from the gravitational effect of the local and global topographical masses so that they all contain both the long- and short-wavelength information. Therefore, the long-wavelength constituent has to be removed, as it is already implicitly included in EGM96. The remaining short-wavelength part is not included (truncated, or omission error) in the GGM, so it should be added. The spectral separation is done via a surface spherical harmonic expansion of the corresponding parameters up to

N_{max} = 360. These effects define the corresponding long-wavelength parts given by the surface spherical harmonic synthesis formulae

$$\delta g_{SDEM}^{N_{\max}}(\Omega,H) = \sum_{n=0}^{N_{\max}} \sum_{m=-n}^{n} \delta g_{SDEM,nm} Y_{nm}(\Omega) \tag{5a}$$

$$\delta g_{0,SDEM}^{N_{\max}}(\Omega,H) = \sum_{n=0}^{N_{\max}} \sum_{m=-n}^{n} \delta g_{0,SDEM,nm} Y_{nm}(\Omega) \tag{5b}$$

$$\delta V_{0,SDEM}^{N_{\max}}(\Omega) = \sum_{n=0}^{N_{\max}} \sum_{m=-n}^{n} \delta V_{0,SDEM,nm} Y_{nm}(\Omega) \tag{5c}$$

$$\delta N_{SDEM}^{N_{\max}}(\Omega) = \sum_{n=0}^{N_{\max}} \sum_{m=-n}^{n} \delta N_{SDEM,nm} Y_{nm}(\Omega) = \frac{\delta V_{0,SDEM}^{N_{\max}}(\Omega)}{\gamma_{ell}} \tag{5d}$$

where $\delta g_{SDEM,nm}$, $\delta g_{0,SDEM,nm}$, $\delta V_{0,SDEM,nm}$ and $\delta N_{SDEM,nm}$ are the fully-normalized spherical harmonic coefficients (degree *n*, order *m*) of $\delta g_{SDEM}(\Omega,H)$, $\delta g_{0,SDEM}(\Omega)$, $\delta V_{0,SDEM}(\Omega)$ and $\delta N_{SDEM}(\Omega)$, respectively, and

$$Y_{nm}(\Omega) = \begin{cases} P_{nm}(\cos\theta)\cos m\lambda & m \geq 0 \\ P_{n|m|}(\cos\theta)\cos|m|\lambda & m < 0 \end{cases}$$

are the surface spherical harmonics (e.g. Heiskanen and Moritz 1967). Each parameter in Eqs (5a) to (5d) is expressed explicitly by a separate surface spherical harmonic expansion. This is in contrast to the usual application of Meissl's spectral scheme (e.g., Rummel and van Gelderen 1995) on the disturbing potential of the Earth's gravity field, which cannot be applied here to derive a surface spherical harmonic expansion of the gravitational attraction due to the topographic masses [cf. Eqs. (5a) and (5b)]. Using Eqs. (5a) to (5d) the short-wavelength parts of the corresponding parameters are given by

$$\delta g_{SDEM}^{>N_{\max}}(\Omega,H) = \delta g_{SDEM}(\Omega,H) - \delta g_{SDEM}^{N_{\max}}(\Omega,H) \tag{6a}$$

$$\delta g_{0,SDEM}^{>N_{\max}}(\Omega) = \delta g_{0,SDEM}(\Omega) - \delta g_{0,SDEM}^{N_{\max}}(\Omega) \tag{6b}$$

$$\delta V_{0,SDEM}^{>N_{\max}}(\Omega) = \delta V_{0,SDEM}(\Omega) - \delta V_{0,SDEM}^{N_{\max}}(\Omega) \tag{6c}$$

$$\delta N_{SDEM}^{>N_{\max}}(\Omega) = \delta N_{SDEM}(\Omega) - \delta N_{SDEM}^{N_{\max}}(\Omega) = \frac{\delta V_{0,SDEM}^{>N_{\max}}(\Omega)}{\gamma_{ell}} \tag{6d}$$

where the superscript $>N_{max}$ indicates parameters with the spectral constituent related to spherical harmonic degrees and orders greater than N_{max} (here, 360)

It should be mentioned that the application of Eqs. (5a-d) and (6a-d) implicitly assume a harmonic continuation between values given at the Earth's surface and the geoid. However, this is only critical if functional values between these two surfaces are of interest, which is not the case here. Furthermore, $\delta g_{SDEM}(\Omega, H)$ has to be expressed in solid spherical harmonics rather than surface spherical harmonics because the 3D functional $\delta g_{SDEM}(\Omega, H)$ is not given as a surface function on the sphere (e.g., the geoid in spherical approximation is used here only for the purpose of applying surface spherical harmonic analysis). However, as long as there exists a one-to-one correspondence between the coordinates of points at the simulated Earth's surface and the spherical polar coordinates (which is the case for AusSEGM), the above spectral separation can be achieved using surface spherical harmonics (e.g., Jekeli 1988).

Here, this relationship can be formulated between the gravitational attraction of the topographical masses evaluated at the simulated Earth's surface $\delta g_{SDEM}(\Omega, H)$ and the geoid $\delta g_{0,SDEM}(\Omega)$. This can be verified by the difference

$$\Delta\delta g_{SDEM}(\Omega, H) = \delta g_{SDEM}(\Omega, H) - \delta g_{0,SDEM}(\Omega), \tag{7}$$

which can be expressed by surface spherical harmonics. Based on Eq. (7), the corresponding fully normalized surface spherical harmonic coefficients are given by

$$\delta g_{SDEM,nm} = \delta g_{0,SDEM,nm} + \Delta\delta g_{SDEM,nm} \tag{8}$$

where $\Delta\delta g_{SDEM,nm}$ are the fully-normalized spherical harmonic coefficients of $\Delta\delta g_{SDEM}(\Omega, H)$ given as a surface function on the geoid.

In order to perform the surface spherical harmonic analysis of the parameters given above (Eqs. 5a-d), the information was extended globally using the same procedure as given above but using the topographical masses as given by JGP95E only. This was done for a coarser resolution for all locations outside the AusSEGM area. Adding globally distributed data provides a smooth transition at the edge of the AusSEGM area, and thus avoids the Gibbs phenomenon. Our earlier experiments indicated that this is an essential requirement; otherwise spurious long-wavelength effects of up to several metres occur in the synthetic geoid near the edge of the AusSEGM area.

The short-wavelength part $\delta g_{SDEM}^{>N_{\max}}(\Omega, H)$ of the gravitational acceleration at the simulated Earth's surface is illustrated in Fig. 7, which mostly shows the behaviour of a spectral resolution of degree and order 360. However, more detail (short-wavelength constituents) can be seen over mountainous areas (rather than flat areas), which is due to the selection of the fractal surface (Section 3). This shows a correlation with the local topography (cf. Figs. 7 and 2), as expected. The magnitude is mostly less than 20 mGal (99.3% of all values) except for high mountainous areas.

Figure 7 near here

The short-wavelength part of the synthetic gravitational potential at the geoid $\delta V_{SDEM}^{>N_{\max}}(\Omega)$ caused by the local and global topographical masses is illustrated in Fig. 8, which shows some correlation with the local topography (Fig. 2) as the highest values are concentrated in mountainous areas. This potential was converted into a synthetic geoidal height (or equivalently a change of the equipotential surface $W=W_0$) $\delta N_{SDEM}(\Omega)$ using Bruns's formula (Eq. 4). The short-wavelength effect on the synthetic geoidal height is generally less than a couple of decimetres (99.4% of all values are less than 0.2 m) with the

largest magnitude of about 0.7 m in areas of highest elevation (cf. Fig. 8 scaled by one order of magnitude).

Figure 8 near here

These short-wavelength AusSEGM geoid and gravity values are very similar to the residual gravity anomalies and residual geoid undulations computed for the AUSGeoid98 regional gravimetric geoid model (Featherstone et al. 2001), indicating both that the prior removal of the long-wavelength components is necessary and that the AusSEGM is realistic. The proof of its realism will be shown in Section 5 using observational data.

4.3 The final AusSEGM

AusSEGM is given by the superposition of the long- and short-wavelength parts for the gravitational acceleration on the simulated Earth's surface and the effect on the geoidal height (change of gravitational potential) over Australia. The free-air anomalies, as well as point gravity values, from AusSEGM are evaluated on the simulated Earth's surface by

$$\Delta g_{SEGM}(\Omega,H) = \Delta g_{GGM}^{N_{\max}}(\Omega,H) + \delta g_{SDEM}^{>N_{\max}}(\Omega,H) \tag{9}$$

$$g_{SEGM}(\Omega,H) = g_{GGM}^{N_{\max}}(\Omega,H) + \delta g_{SDEM}^{>N_{\max}}(\Omega,H), \tag{10}$$

respectively. Furthermore, the AusSEGM geoidal heights are given by

$$N_{SEGM}(\Omega) = N_{GGM}^{N_{\max}}(\Omega) + \delta N_{SDEM}^{>N_{\max}}(\Omega). \tag{11}$$

Using the above approach, point gravity values on the simulated Earth's surface and geoidal heights were simulated at uniform 1-arc-min by 1-arc-min grid nodes over Australia. In addition, gravity values were also simulated at discrete points on the topography, which are distributed according to the way in which gravity data are collected in the field. This creates a gravity data set that reflects the usual situation in gravimetric

geoid computation. For instance, in mountainous regions, gravity observations tend to be made in the more accessible lowland regions (e.g., valleys).

The horizontal positions of these simulated point gravity observations were driven by actual gravity observations over Australia in an efficient way by taking the simulated gravity value from the 1-arc-min grid (~1.8 km) that is nearest to an actual gravity observation (Fig. 9). Furthermore, the height of all 330,929 simulated point gravity values is taken from the 3-arc-sec SDEM, so that each point is located on the simulated Earth's surface at the centre of a SDEM element.

Figure 9 near here

Table 2 shows a statistical summary of the AusSEGM-generated gravity as well as free-air gravity anomalies at the simulated Earth's surface and the AusSEGM-generated geoidal heights. Since these data have been derived using the same input data, they are entirely consistent with each other. It is essential to note that the synthetic gravity observations on the topography have **not** been used here to compute the synthetic geoid, e.g., via Stokes's integral. This is deliberate because the primary aim of AusSEGM is to test the computation of a gravimetric geoid model using the simulated data.

Table 2 near here

5 Comparison of AusSEGM with real data over Australia

In order to demonstrate that AusSEGM provides realistic gravity field estimates, the AusSEGM-generated gravity values on the SDEM surface have been compared with a subset of 330,929 measured gravity stations supplied by Geoscience Australia

(http://www.ga.gov.au/oracle/index.jsp; Fig. 9). As the measured and simulated gravity stations are not at exactly the same locations, differences are expected. No correction for the horizontal offset has been applied, but a correction (the free-air gradient) has been applied for the height difference between the observation elevation and the SDEM surface (simulated Earth's surface).

This comparison shows a reasonably good agreement (Fig. 10) as most of the differences are less than 20 mGal (99.3% of all values), and the spatial distribution shows no significant trend (e.g., linear regression of the difference with respect to latitude yields: +0.48 mGal/degree with a low correlation coefficient of 0.25). Therefore, it can be claimed that AusSEGM indeed provides realistic simulated values of the gravity field of the Earth.

Figure 10 near here

Furthermore, the AusSEGM-generated geoidal heights have been compared with 254 co-located GPS ellipsoidal heights and spirit-levelled heights on the Australian Height Datum (AHD). These data were provided by Geoscience Australia, and supersede the GPS-AHD data used by Featherstone et al. (2001). This comparison has been included despite the problems mentioned in the Introduction. As such, it only serves to demonstrate that AusSEGM reproduces the general structure of the geoid over Australia.

This comparison (Fig. 11) shows a mean difference of ~1 m (no bias has been removed here), which is roughly equal to the zero-degree term computed for AUSGeoid98 (Featherstone et al. 2001). However, there is a substantial ~2-m north-south trend in the differences in Fig. 11 (linear regression of the difference with respect to latitude yields: ~+0.026 m/degree with a correlation coefficient of 0.58). This is mostly due to distortions

in the AHD invoked by fixing the heights of 32 tide gauges to zero in its realisation (Roelse et al. 1971), thus neglecting to account for the general north-south trend in sea surface topography around Australia (cf. Featherstone 2002a, 2004).

Figure 11 near here

This is a significant by-product result because no significant (correlation coefficient 0.25) north-south trend is evident in the comparisons between AusSEGM and the Australian gravity observations (Fig. 10), so the north-south trend must be in the AHD (there is no documented evidence of north-south trends in GPS ellipsoidal heights). Featherstone (2004) points out the problem of separating levelling and gravimetric geoid errors in GPS-AHD comparisons, but the use of the AusSEGM has avoided this. As such, AusSEGM has found another application by adding to the body of evidence of the distortions in the AHD (cf. Roelse et al. 1971; Featherstone 2002a). However, it should be stressed here that the primary aim of an SEGM is not to check for errors in gravity or levelling data. This should only be done if the SEGM is proven to be good representation of reality. In this case, it can be helpful in the interpretation of results obtained elsewhere.

Finally, the power spectrum of AusSEGM does not show any discontinuity between the long- and short-wavelength contributions at spherical harmonic degree N_{max} = 360, but rather shows a seamless extension of the [global] spectral content of EGM96. This can be seen in Fig. 12, which shows the degree variances for the geoid height, where the long-wavelength constituents (degrees up to and including N_{max} = 360) are taken from EGM96 and the short-wavelength constituents (degrees beyond N_{max}=360) are from AusSEGM. The degree variances beyond N_{max} = 360 were determined from the 2D power spectral density (PSD) function outlined in Schwarz (1984). Therefore, it is not necessary

to enforce a smooth transition on the power spectrum of AusSEGM, as is sometimes applied to other combined source-effect SEGMs (e.g., Haagmans 2000, Claessens 2003).

Figure 12 near here

6 Reference level of the DEMs

In the above procedure to compute AusSEGM, the question arises if the procedure should be iterative or not. It has been assumed throughout this manuscript that all DEM elevations refer to the long-wavelength spheroid defined by EGM96. Clearly, the DEMs add short-wavelength variations to EGM96 to produce the AusSEGM geoid (Fig. 8 divided by normal gravity γ (i.e., approximately one order of magnitude)). Therefore, strictly speaking, the SDEM should be referred to the AusSEGM geoid and not to EGM96. At the beginning, however, AusSEGM is unknown.

Considering this, the question arises of an iterative procedure is directly related to whether SDEM heights (and therefore the topographic masses as well) change due to the additional short-wavelength AusSEGM geoid undulations. This question can be studied by the relationship $N \doteq h - H$, where h is the ellipsoidal height. If short-wavelength variations are added to N, either h changes and H is preserved (see Section 6.1) or vice versa H changes and h is preserved (see Section 6.2). These situations are illustrated in Fig. 13.

Figure 13 near here

6.1 SDEM heights are preserved

In this case, the short-wavelength synthetic geoid variations caused by the topographic masses are added to the initially assumed geoidal height $N_{EGM96}^{N_{max}}$, and H is assumed to remain unchanged. Thus, the ellipsoidal height h will be changed by $\delta N_{SDEM}^{>N_{max}}$. This means that the topographic masses remain unchanged apart from a slight vertical shift (up or down) according to the added short-wavelength variations (Fig. 13b).

Here, for the purpose of determining the topographic effect on potential and gravity only, the topographic masses (defined by H) have been assumed to refer to a mean sphere, which approximates the EGM96 spheroid. It has been estimated that the difference in the short-wavelength effect of the gravitational attraction whether the topographic masses (DEM height H) are referred to a mean sphere or ellipsoid remains well below 10 μGal for the gravitational attraction. Following this approach, a possible second iteration will provide no further contribution as the topographic masses remain unchanged and will be referred to the same mean sphere (or ellipsoid) as used in the first iteration step. In this case, no iteration is necessary. However, the free-air gravity anomaly as given by the GGM will change slightly, as the height above ellipsoid has been changed by the amount of the short wavelength part on the geoidal height $\delta N_{SDEM}^{>N_{max}}$. This effect will reach a maximum of 1 μGal for a maximum height change of 1 m (cf. Fig 8 divided by about 10).

6.2 SDEM heights are not preserved

As opposed to the previous section, h in this case remains unchanged and the DEM height H is changed by the amount of the short-wavelength geoid variation $\delta N_{SDEM}^{>N_{max}}$ (Fig. 13 c). This results in a direct change of the topographic masses and accordingly a further contribution to the effects on the gravitational potential and attraction; thus, iteration

becomes necessary. In the case of AusSEGM, the topographical height taken in a second iteration step changes by an amount of less than 1 m (cf. Fig 8 divided by ~10). The corresponding gravitational effect has been studied for a smaller sample area, which includes the highest SDEM elevation over Australia (2405.4 m; Fig. 3).

The effect on gravitational attraction and potential due to a second iteration step reaches maximum values of 30 μGal for a change in gravitational attraction and 3 mm for a change in the geoidal height. Given these small changes, there is no need for further iteration regarding our specified precision level of better than 1 cm for the AusSEGM geoidal height. These values are extreme because the computations were performed for the maximum height of the Australian SDEM. Of course, larger values will occur in cases where a regional SEGM is developed in areas of larger elevations.

The maximum values of 30 μGal and 3 mm for the gravitational attraction and geoidal height, respectively, can be taken as a precision measure for AusSEGM after the first iteration (i.e., no additional correction for the change in synthetic geoid reference surface for the SDEM). This precision is acceptable for validation of geoid determination theories, techniques and computer software with the aim of a 1 cm geoid. If iteration is considered, then the precision of AusSEGM can be taken to be 1 mm and 1 μGal or better for the geoidal height and gravity values, respectively.

7. Summary and Conclusions

This paper has described the construction of a regional high-resolution (1-arc-minute, ~1.8 km), synthetic Earth gravity model (SEGM) over Australia (AusSEGM). The AusSEGM provides gravity values and free-air gravity anomalies at the simulated Earth's surface, given by a synthetic digital elevation model (SDEM), and self-consistent geoidal heights. The former are the basic input data for regional gravimetric geoid computation over land

areas, and are provided as Electronic Supplementary Material (ESM) with this paper. Gravity data are given on a regular grid (1-arc-min by 1-arc-min) and at discrete points that are distributed according to the way in which gravity data are usually collected in the field. The accuracy of the synthetic gravity and geoid data (after a first iteration) is estimated to be better than 30 μGal and 3 mm, respectively.

AusSEGM is a combined source-effect model including a high-resolution (3-arc-sec by 3-arc-sec) SDEM derived from the GLOBE v1 global DEM using a realistic fractal surface. The long-wavelength constituent (up to spherical harmonic degree $N_{max} = 360$) of AusSEGM is taken from an assumed error-free EGM96 (effect part), whereas the short-wavelength part beyond $N_{max} = 360$ over Australia is taken from the gravitational effects calculated by Newtonian forward modelling from the SDEM (source part). The spectral separation has been done using surface spherical harmonic analysis at degree 360. The contribution of the short-wavelength source part is generally small and remains in most cases (more than 99% of all values) under 0.2 m and 20 mGal for the geoidal height and gravitational acceleration, respectively.

A comparison of AusSEGM-generated gravity data with gravity observations over Australia shows that it reproduces the actual gravity field very well; most differences (91.2%) are less than 20 mGal. Furthermore, a comparison of AusSEGM geoidal heights with GPS and AHD data shows a standard deviation of 0.32 m, but also helps confirm that there is a dominant north-south slope in the AHD. Overall, AusSEGM is realistic and can be regarded as well suited for any gravity field study over Australia. Importantly, all data are consistent with each other as they use the same input data and therefore can be used to validate regional geoid determination theories, techniques and computer software. This will be demonstrated in a further study.

Acknowledgements: This research was funded by the Australian Research Council (ARC) through the large grant A00001127 to Will Featherstone and Petr Vaníček. Gary Johnston at Geoscience Australia kindly provided the GPS-levelling data. Grateful thanks go to Roland Pail and two unknown reviewers for their helpful suggestions and comments on this paper. Furthermore, the authors would like to acknowledge Zdeněk Martinec who brought up this idea in the mid 1990s.

References

Adler RJ (1981) The geometry of random fields, Wiley, New York, 280 pp

Ågren J (2004) Regional geoid determination methods for the era of satellite gravimetry: numerical investigations using synthetic Earth gravity models, doctoral dissertation, Department of Infrastructure, Royal Institute of Technology (KTH), Stockholm, 246pp

Claessens SJ (2003) A synthetic Earth model, Delft University Press, Delft, 61pp

Dziewonski AM, Anderson DL (1981) Preliminary reference Earth model, Physics of the Earth and Planetary Interiors 25(4): 297-356

Ellman A (in press) Two deterministic and three stochastic modifications of Stokes's formula: a case study for the Baltic countries, J Geod, doi: 10.1007/s00190-005-0438-1

Featherstone WE (1999) Progress Report for IAG SSG3.177 Synthetic modelling of the Earth's gravity field, in: Anderson OB (ed) International Association of Geodesy, Travaux http://www.gfy.ku.dk/~iag/Travaux_99/ssg3177.htm

Featherstone WE (2002a) Prospects for the Australian height datum and geoid model, in: Adam J, Schwarz K-P (eds) Vistas for Geodesy in the New Millennium, Springer, Berlin Heidelberg New York, pp 96-101

Featherstone WE (2002b) Tests of two forms of Stokes's integral using a synthetic gravity field based on spherical harmonics. In: Grafarend EW, Krumm FW, Schwarze VS (eds), Geodesy - The Challenge for the Third Millennium, Springer, Berlin Heidelberg New York, pp 163-171

Featherstone WE (2004) Evidence of a north-south trend between AUSGeoid98 and the AHD in southwest Australia, Survey Review 37(291): 334-343

Featherstone WE, Olliver JG (1997) A method to validate gravimetric geoid computation software based on Stokes's integral, J Geod 72(3): 154-160, doi: 10.1007/s001900050125

Featherstone WE, Kirby JF, Kearsley AHW, Gilliland JR, Johnston GM, Steed J, Forsberg R, Sideris MG (2001) The AUSGeoid98 geoid model of Australia: data treatment, computations and comparisons with GPS-levelling data, J Geod 75(5-6): 313-330, doi: 10.1007/s001900100177

Haagmans R (2000) A synthetic Earth model for use in geodesy, J Geod 74(7-8): 503-511, doi: 10.1007/s001900000112

Hastings DA, Dunbar PK (1998) Development & Assessment of the Global Land One-km Base Elevation Digital Elevation Model (GLOBE), ISPRS Archives, 32(4): 218-221 http://www.ngdc.noaa.gov/mgg/topo/globe.html

Heiskanen WA, Moritz H (1967) Physical geodesy, W H Freeman and Co, San Francisco

Hilton RD, Featherstone WE, Berry PAM, Johnston CPD, Kirby JF (2003) Comparison of digital elevation models over Australia and external validation using ERS-1 satellite radar altimetry, Australian Journal of Earth Sciences 50(2): 157-168, doi: 10.1046/j.1440-0952.2003.00982.x

Hutchinson M (2001) GeoData 9 second DEM Version 2: A digital elevation model of Australia with a grid spacing of nine seconds in longitude and latitude. Data User

Guide, 2nd ed., Geoscience Australia, Canberra, Australia, 43 pp http://www.ga.gov.au/image_cache/GA4783.pdf

Jekeli C (1988) The exact transformation between ellipsoidal and spherical harmonic expansions. manuscripta geodaetica 13(2): 106-113

Kuhn M (2003) Geoid determination with density hypotheses from isostatic models and geological information, J Geod 77(1-2): 50-65, doi: 10.1007/s00190-002-0297-y

Kuhn M, Seitz K (2005) Evaluation of Newton's integral in space and frequency domain. in: Sansò, F. (ed) A Window on the Future of Geodesy, Springer, Berlin Heidelberg New York, pp

Kuhn M, WE Featherstone (2005) Construction of a synthetic Earth gravity model by forward gravity modelling, in: Sansò, F. (ed) A Window on the Future of Geodesy, Springer, Berlin Heidelberg New York, pp 350-355

Kuroishi Y, Ando H, Fukuda Y (2002) A new hybrid geoid model for Japan, GSIGEO2000, J Geod 76(8): 428-436, doi: 10.1007/s00190-002-0266-5

Lemoine FG, Kenyon SC, Factor JK, Trimmer RG, Pavlis NK, Chinn DS, Cox CM, Klosko SM, Luthcke SB, Torrence MH, Wang YM, Williamson RG, Pavlis EC, Rapp RH, Olson TR (1998) The development of the joint NASA GSFC and the National Imagery and Mapping Agency (NIMA) geopotential model EGM96, NASA/TP-1998-206861, Goddard Space Flight Center, National Aeronautics and Space Administration, Greenbelt

Moritz H (1980) Advanced physical geodesy, Herbert Wichman, Karlsruhe, Germany, 497pp

Nahavandchi H, Sjöberg LE (2001) Precise geoid determination over Sweden using the Stokes-Helmert method and improved topographic corrections, J Geod 75(2-3): 74-88, doi: 10.1007/s001900000154

Novák P, Vaníček P, Véronneau M, Holmes S, Featherstone WE (2001) On the accuracy of modified Stokes's integration in high-frequency gravimetric geoid determination, J Geod 74(11): 644-654, doi: 10.1007/s001900000126

Pail R (2000) Synthetic global gravity model for planetary bodies and applications in satellite gravity gradiometry, PhD thesis, Technical University of Graz, Graz

Roelse A, Granger HW, Graham JW (1971) The adjustment of the Australian levelling survey 1970-1971, Tech Rep 12, Division of National Mapping, Canberra, 81pp

Rummel R, Rapp HR, Sünkel H (1988) Comparison of global topographic/isostatic models to the Earth's observed gravity field, Rep 388, Dept Geod Sci and Surv, Ohio State Univ, Columbus, 33pp

Rummel R, van Gelderen M (1995) Meissl scheme - spectral characteristics of physical geodesy, manuscripta geodaetica 20(5): 379-385

Schwarz KP (1984) Data types and their spectral properties. In Schwarz, K-P. (ed.): Local Gravity Field Approximation, Proc Int Summer School, Beijing, pp 1-66

Smith DA, Roman DR (2001) GEOID99 and G99SSS: 1-arc-minute geoid models for the United States, J Geod 75(9-10): 469-490, doi 10.1007/s001900100200

Tziavos IN (1996) Comparisons of spectral techniques for geoid computations over large regions, J Geod 70(6): 357-373, doi: 10.1007/s001900050027

Vaníček P, Featherstone WE (1998) Performance of three types of Stokes's kernel in the combined solution for the geoid, J Geod 72(12): 684-697, doi: 10.1007/s001900050209

Vaníček P, Kleusberg A (1987) The Canadian geoid - Stokesian approach, manuscripta geodaetica 12(2): 86-98

Vaníček P, Martinec Z (1994) Stokes-Helmert scheme for the evaluation of a precise geoid, manuscripta geodaetica 19(2): 119-128

Véronneau M, SD Pagiatakis, P Vaníček, P Novák, J Huang, J Janák, MG Sideris, O Esan (2000) Canadian Gravimetric Geoid Model 2000 (CGG2000), in Sideris MG (ed) Gravity, Geoid and Geodynamics 2000, Springer, Berlin Heidelberg New York, pp

List of table and figure captions:

Table 1: DEM resolutions and spatial extensions for the practical computation of AusSEGM

Table 2. Descriptive statistics of the AusSEGM parameters

Figure 1: Schematic view of the global (long-wavelength) and local (short-wavelength) components of AusSEGM in the concept of a source-effect SEGM.

Figure 2: The 3-arc-sec by 3-arc-sec simulated DEM (SDEM) over Australia (Mean: 128.2 m, Min: 0.0 m, Max: 2405.4 m, SD: 194.0 m) (Lambert projection).

Figure 3: Differences between SDEM (averaged to 9-arc-sec by 9-arc-sec) and DEM-9S v2 DEM of Australia (Mean: 20.0 m, Min: -516.5 m, Max: 1159.5 m, SD: 61.3 m). The large differences are due to errors in the GLOBE v1 source data; see Hilton et al. (2003).

Figure 4: Synthetic gravitational acceleration at the Earth's surface due to forward modelling of the global topography. (Mean: 51.6 mGal, Min: 14.3 mGal, Max: 246.8 mGal, SD: 22.1 mGal).

Figure 5: Synthetic gravitational acceleration at the synthetic geoid ($H = 0$) due to forward modelling of the global topography. (Mean: -13.9 mGal, Min: -163.2 mGal, Max: 19.3 mGal, SD: 21.1 mGal).

Figure 6: Synthetic gravitational potential at the synthetic geoid (H = 0) due to forward modelling of the global topography. (Mean: 2424.4 m^2/s^2, Min: 2133.9 m^2/s^2, Max: 2647.6 m^2/s^2, SD: 122.1 m^2/s^2).

Figure 7: Short-wavelength component (degrees > 360) of the synthetic gravitational acceleration at the Earth's surface after a surface-spherical-harmonic-based spectral separation (Mean: 0.0 mGal, Min: -88.6 mGal, Max: 125.8 mGal, SD: 5.4 mGal).

Figure 8: Short-wavelength component (degrees > 360) of the synthetic gravitational potential at the synthetic geoid after a surface-spherical-harmonic-based spectral separation (Mean: 0.2 m^2/s^2, Min: -5.6 m^2/s^2, Max: 6.4 m^2/s^2, SD: 0.6 m^2/s^2)

Figure 9: Distribution of 330,929 simulated point gravity observations over Australia.

Figure 10: Comparison of the AusSEGM gravity values with 330,929 measured gravity values over Australia (Mean: -1.0 mGal, Min: -244.2 mGal, Max: 70.4 mGal, SD: 12.0 mGal).

Figure 11: Comparison of the AusSEGM geoidal height with 254 GPS-AHD points (Mean: 0.95 m, Min: 0.05 m, Max: 1.90 m, SD: 0.32 m).

Figure 12: Degree variances (signal power) for the geoid height taken from EGM96 (up to N_{max} = 360) and the PSD of AusSEGM geoid heights (beyond N_{max} = 360).

Figure 13: Schematic illustration of the iterative computation procedure. a) *Initial situation:* Heights H are referred to the geoid given by EGM96. b.) *No iteration:* Heights H are referred to the new synthetic geoid and remain unchanged. The ellipsoid height h is changed by $\delta N_{SDEM}^{N_{max}}$. c.) *Iteration:* Heights H are referred to the new synthetic geoid and are changed by $\delta N_{SDEM}^{N_{max}}$. The ellipsoid height h remains unchanged.

Table 1: DEM resolutions and spatial extensions for the practical computation of AusSEGM

Resolution	**Extension (λ_r, φ_r) or Fixed Boundary**	**Source**
3" x 3"	$\lambda_r = \varphi_r$ = 10-arc-min (variable boundary)	SDEM
15" x 15"	$\lambda_r = \varphi_r$ = 20-arc-min (variable boundary)	SDEM
1' x 1'	$\lambda_r = \varphi_r = 1°$ (variable boundary)	SDEM
5' x 5'	λ: 107°E - 160°E; φ: 3°S - 50°S (fixed boundary)	JGP95E/SDEM
30' x 30'	λ: 102°E - 165°E; φ: 2°N - 55°S (fixed boundary)	JGP95E/SDEM
60' x 60'	Global (fixed boundary)	JGP95E/SDEM

Table 2. Descriptive statistics of the AusSEGM parameters

AusSEGM parameter	Max	Min	Mean	SD
Gravity at the Earth's surface (m/s^2)	9.80528	9.78051	9.78954	0.004372
Free-air gravity anomalies at the Earth's surface (mGal)	190.9	-113.2	1.8	15.8
Geoid heights (m)	72.0	-34.9	6.4	17.5

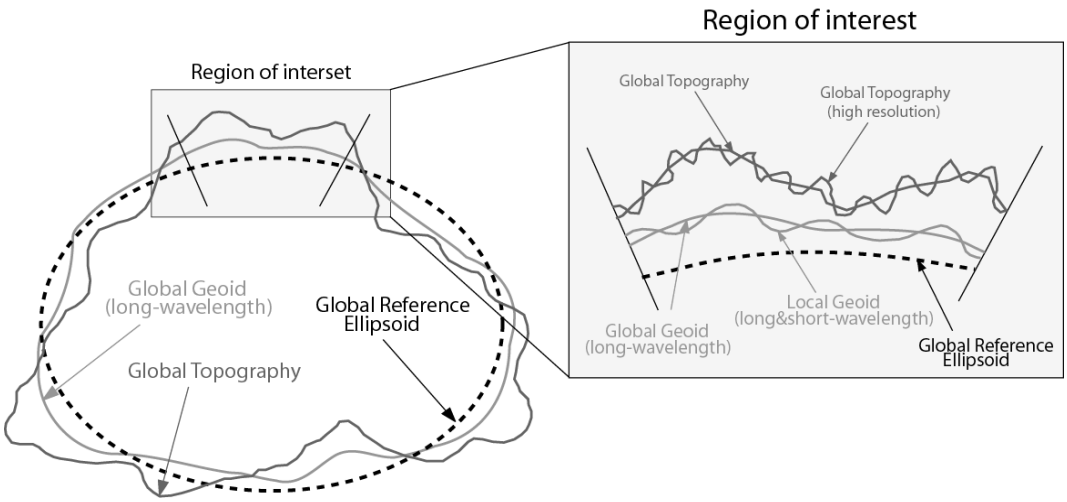

Figure 1: Schematic view of the global (long-wavelength) and local (short-wavelength) components of AusSEGM in the concept of a source-effect SEGM.

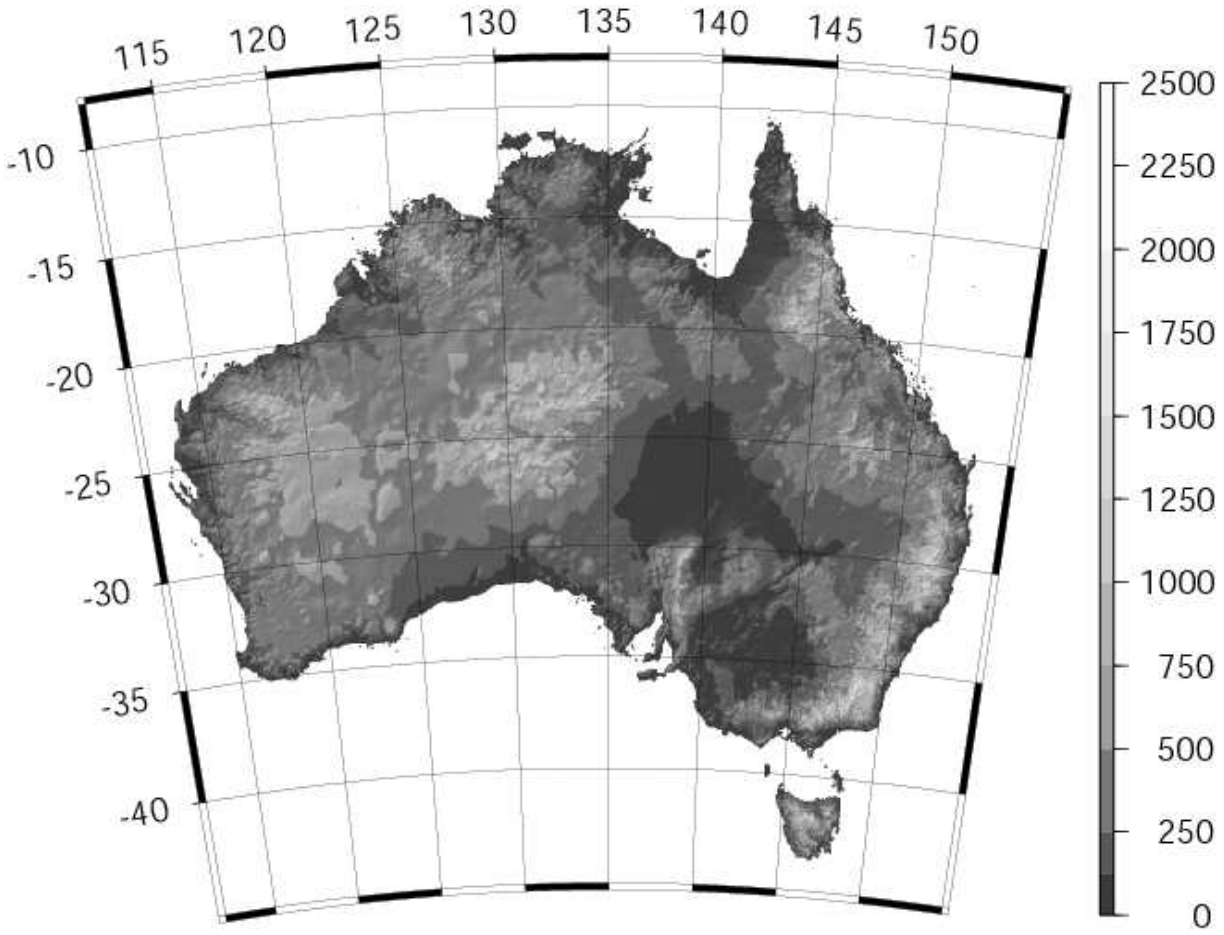

Figure 2: The 3-arc-sec by 3-arc-sec simulated DEM (SDEM) over Australia (Mean: 128.2 m, Min: 0.0 m, Max: 2405.4 m, SD: 194.0 m) (Lambert projection).

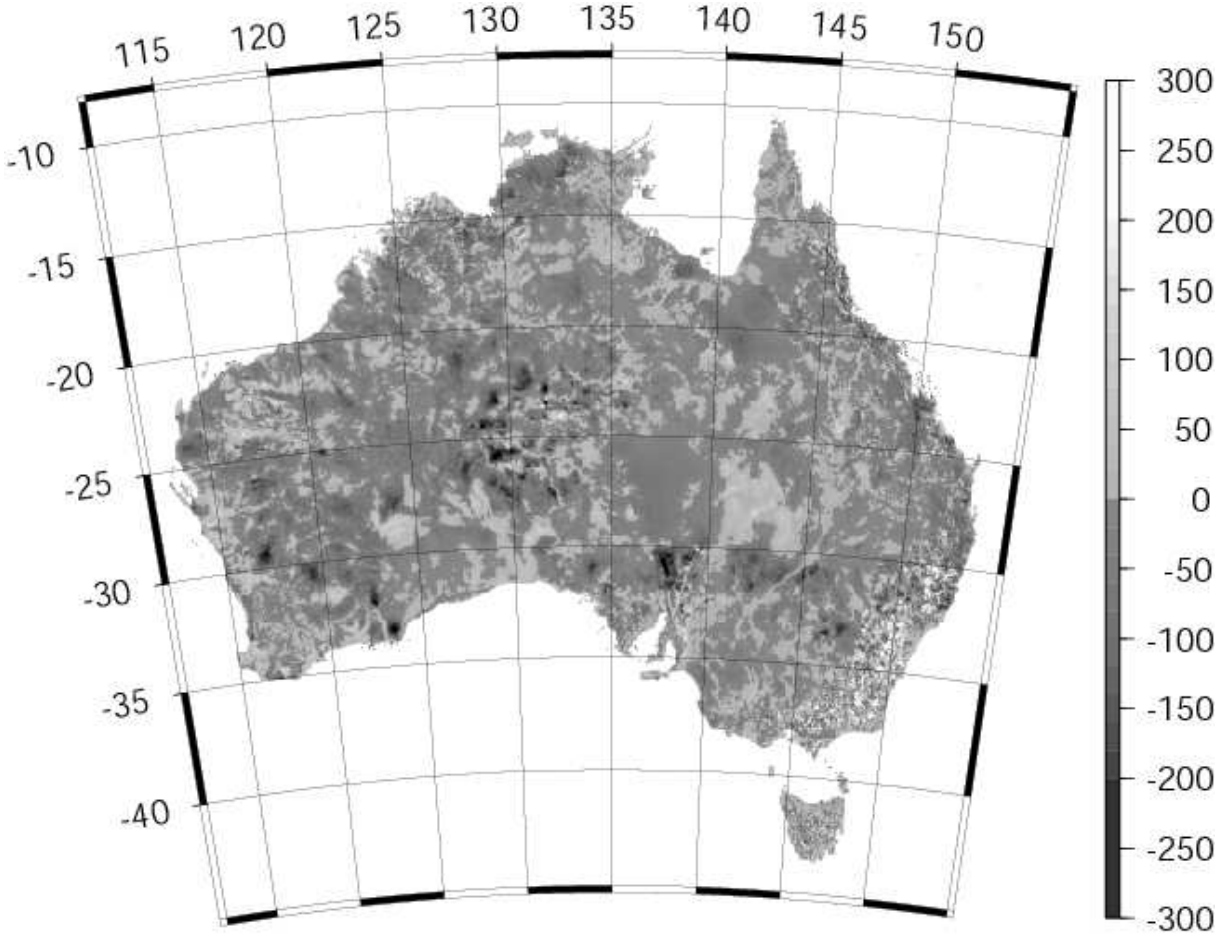

Figure 3: Differences between SDEM (averaged to 9-arc-sec by 9-arc-sec) and DEM-9S v2 DEM of Australia (Mean: 20.0 m, Min: -516.5 m, Max: 1159.5 m, SD: 61.3 m). The large differences are due to errors in the GLOBE v1 source data; see Hilton et al. (2003).

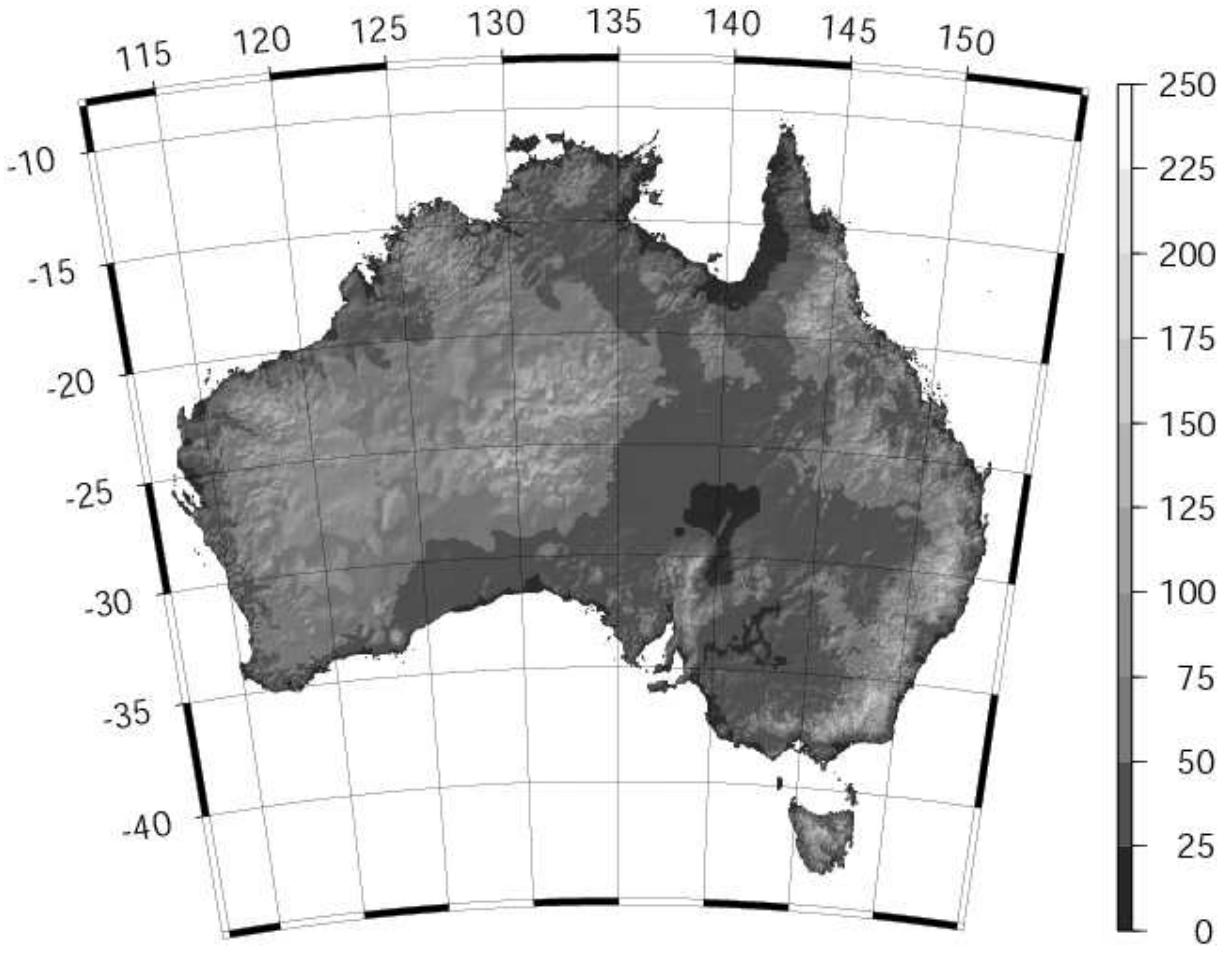

Figure 4: Synthetic gravitational acceleration at the Earth's surface due to forward modelling of the global topography. (Mean: 51.6 mGal, Min: 14.3 mGal, Max: 246.8 mGal, SD: 22.1 mGal).

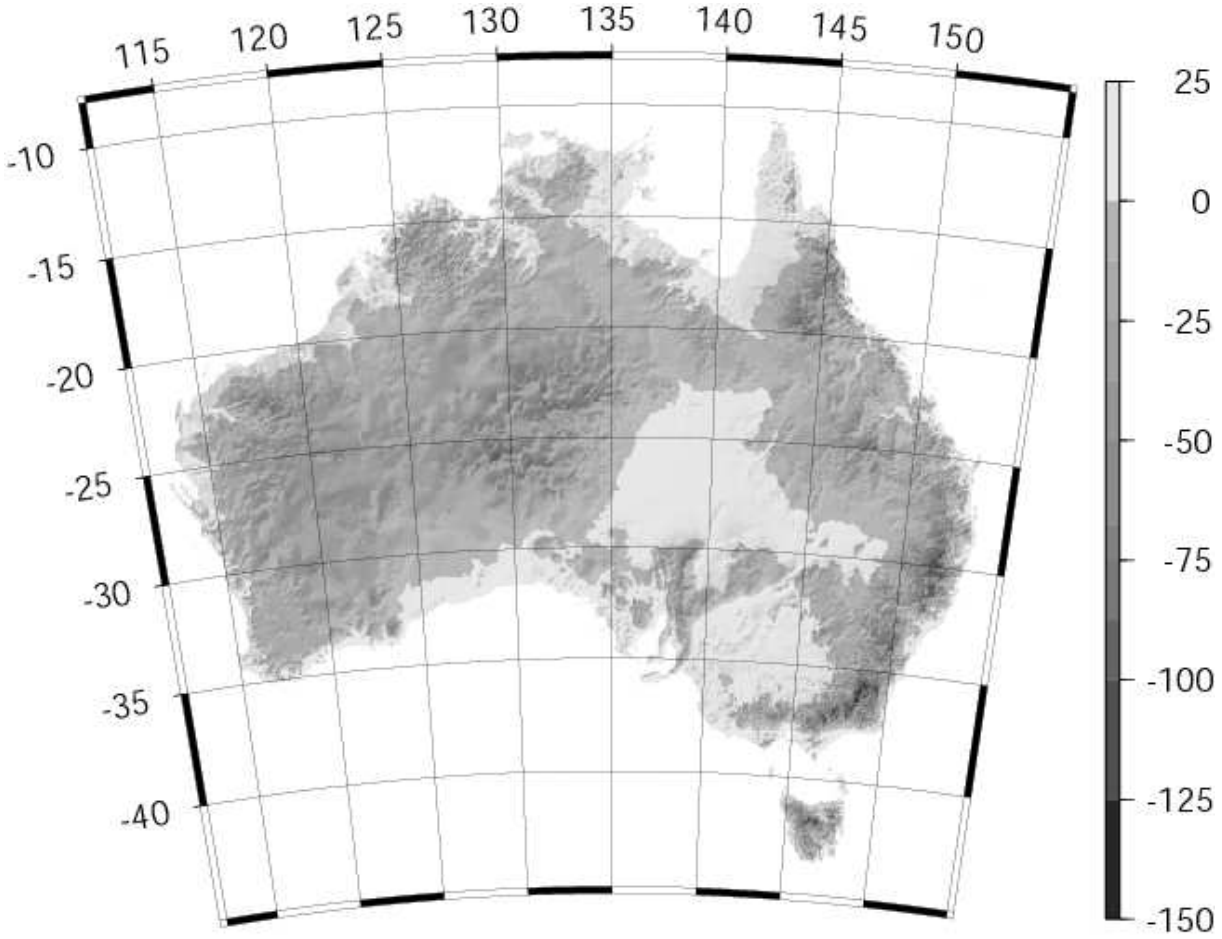

Figure 5: Synthetic gravitational acceleration at the synthetic geoid ($H = 0$) due to forward modelling of the global topography. (Mean: -13.9 mGal, Min: -163.2 mGal, Max: 19.3 mGal, SD: 21.1 mGal).

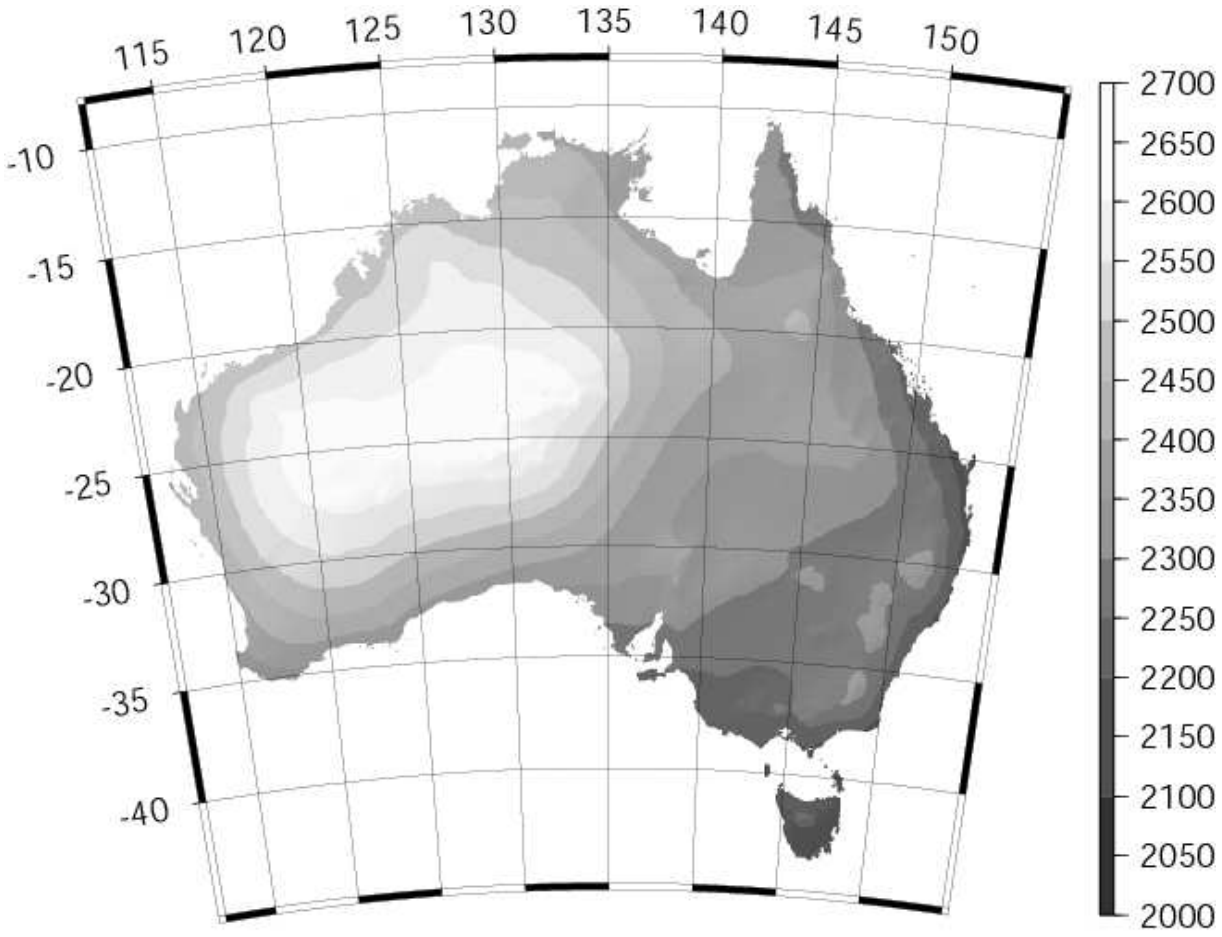

Figure 6: Synthetic gravitational potential at the synthetic geoid ($H = 0$) due to forward modelling of the global topography. (Mean: 2424.4 m^2/s^2, Min: 2133.9 m^2/s^2, Max: 2647.6 m^2/s^2, SD: 122.1 m^2/s^2).

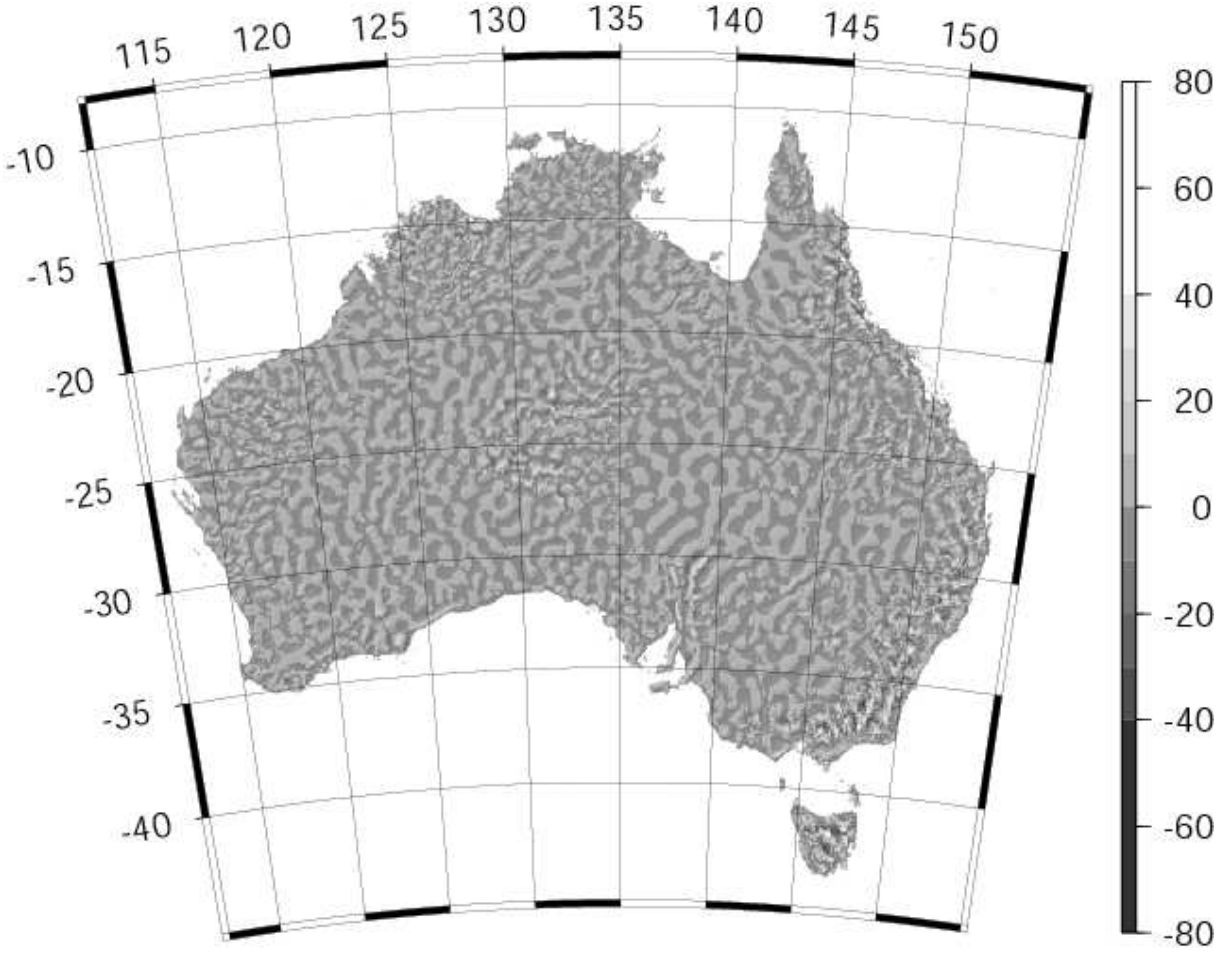

Figure 7: Short-wavelength component (degrees > 360) of the synthetic gravitational acceleration at the Earth's surface after a surface-spherical-harmonic-based spectral separation (Mean: 0.0 mGal, Min: -88.6 mGal, Max: 125.8 mGal, SD: 5.4 mGal).

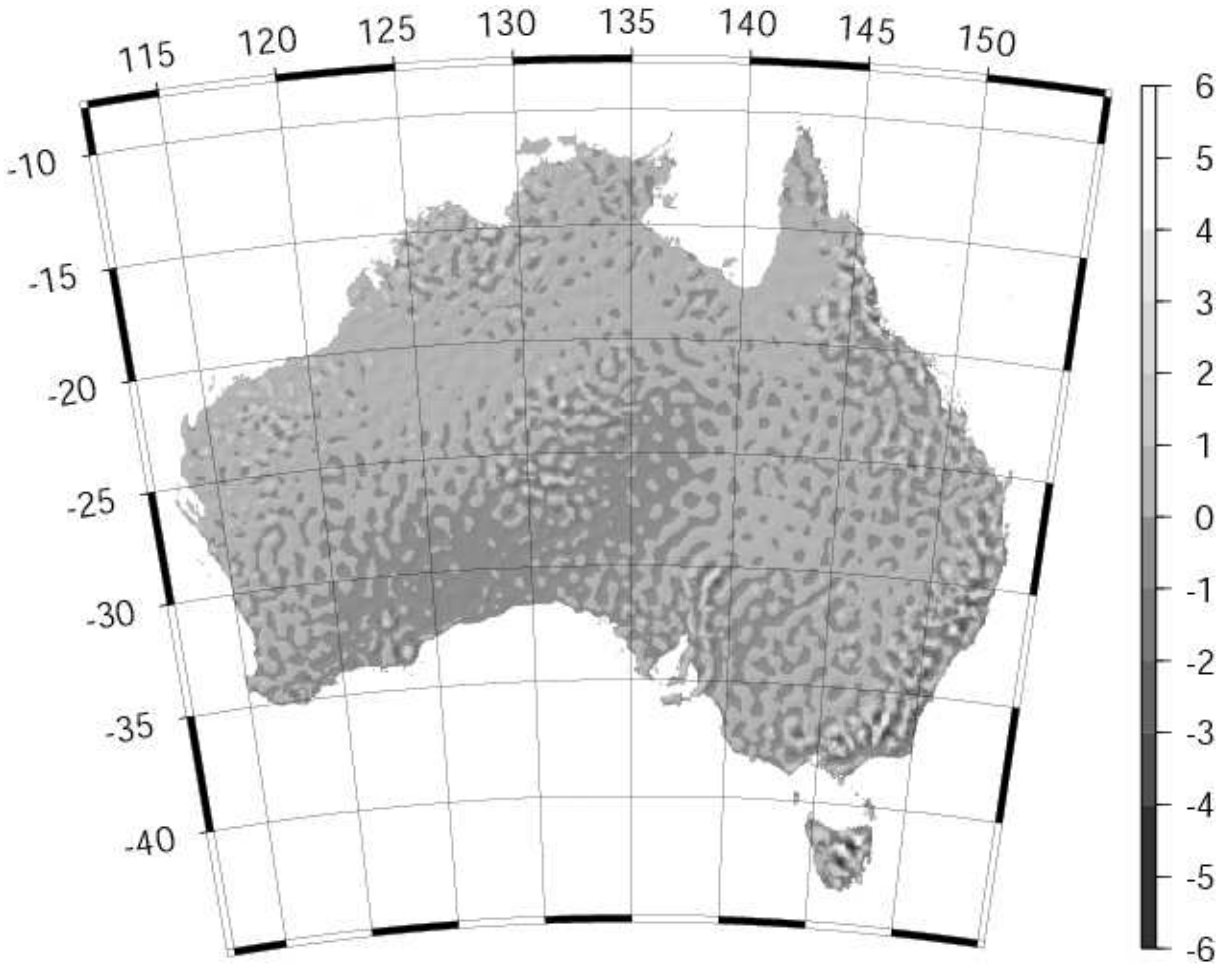

Figure 8: Short-wavelength component (degrees > 360) of the synthetic gravitational potential at the synthetic geoid after a surface-spherical-harmonic-based spectral separation (Mean: 0.2 m^2/s^2, Min: -5.6 m^2/s^2, Max: 6.4 m^2/s^2, SD: 0.6 m^2/s^2)

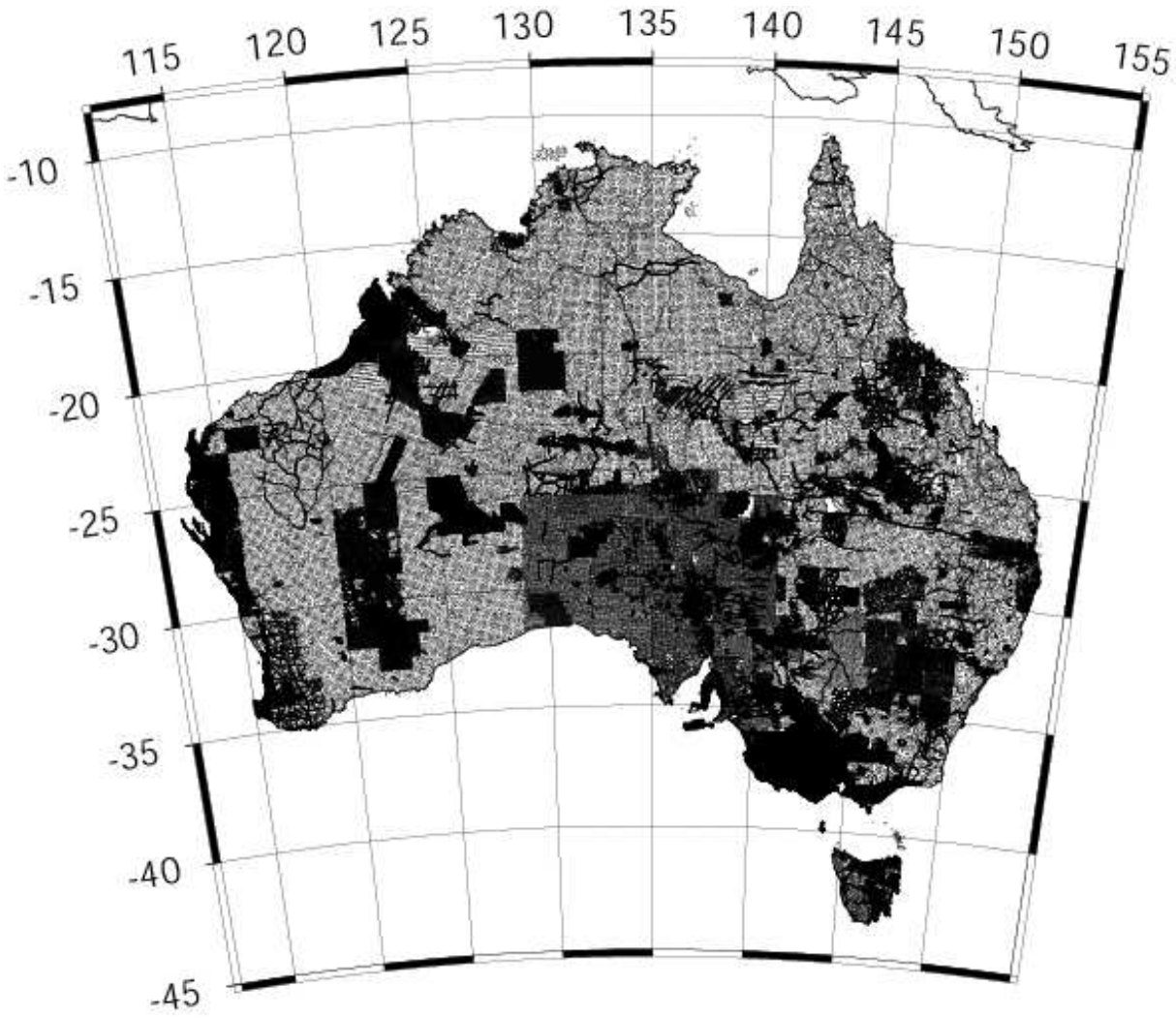

Figure 9: Distribution of 330,929 simulated point gravity observations over Australia.

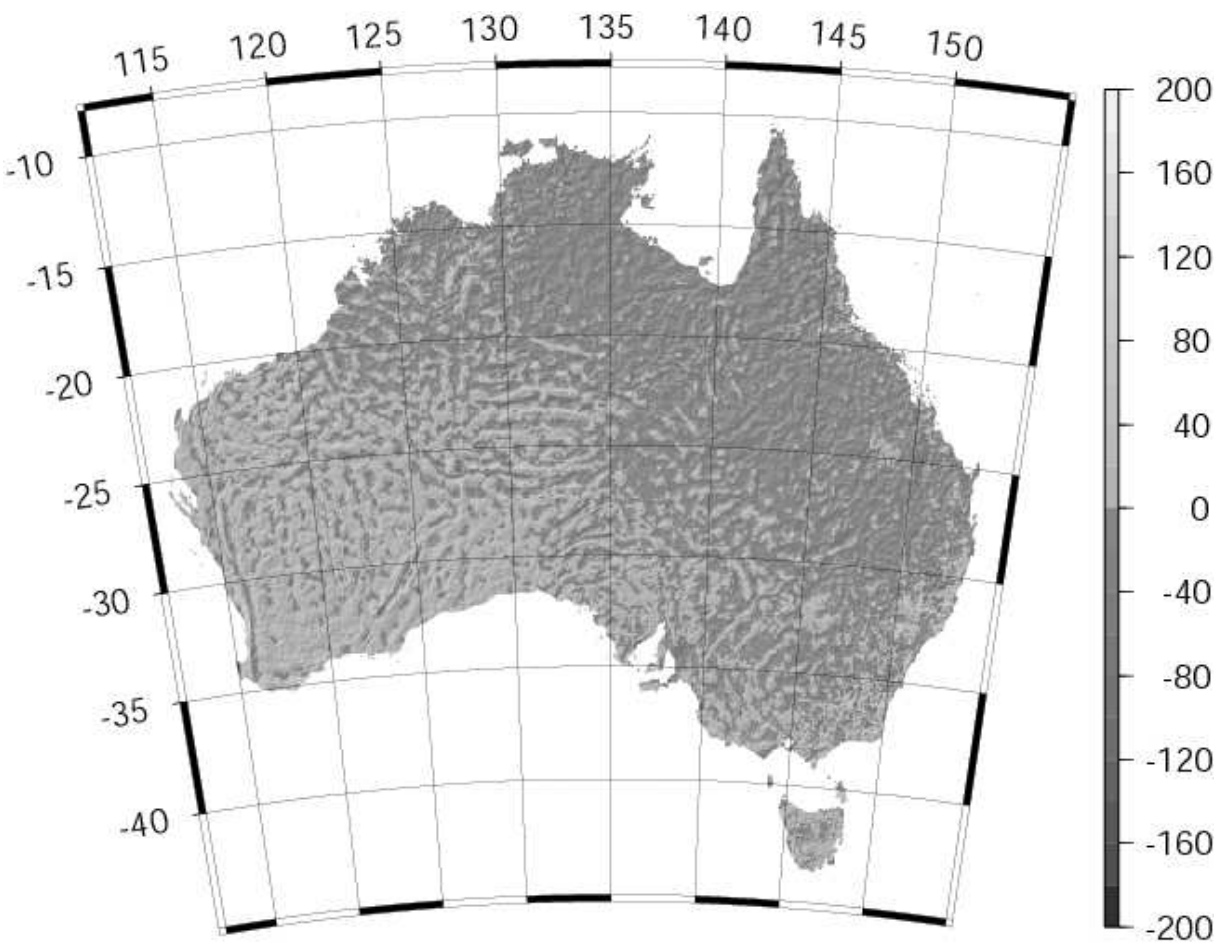

Figure 10: Comparison of the AusSEGM gravity values with 330,929 measured gravity values over Australia (Mean: -1.0 mGal, Min: -244.2 mGal, Max: 70.4 mGal, SD: 12.0 mGal).

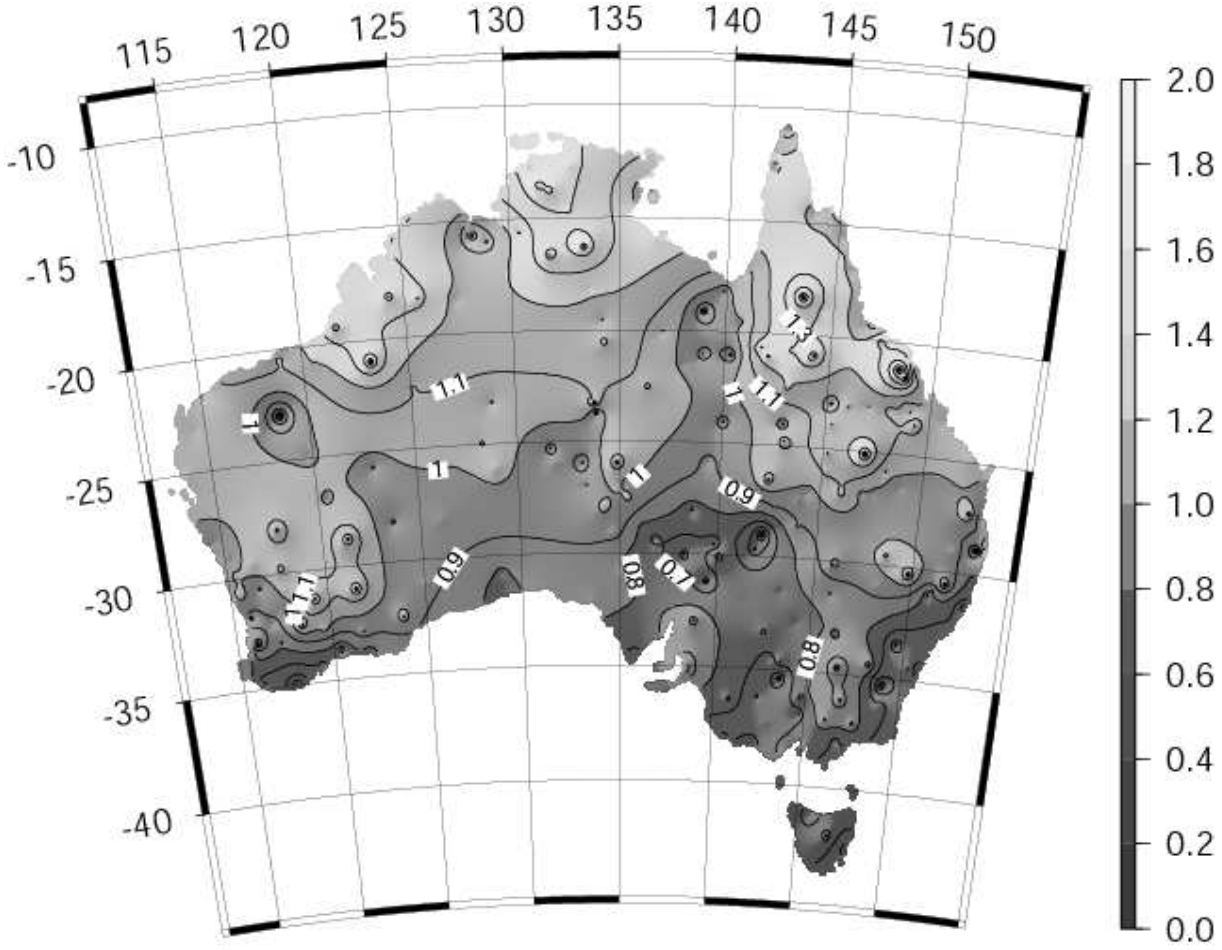

Figure 11: Comparison of the AusSEGM geoidal height with 254 GPS-AHD points (Mean: 0.95 m, Min: 0.05 m, Max: 1.90 m, SD: 0.32 m).

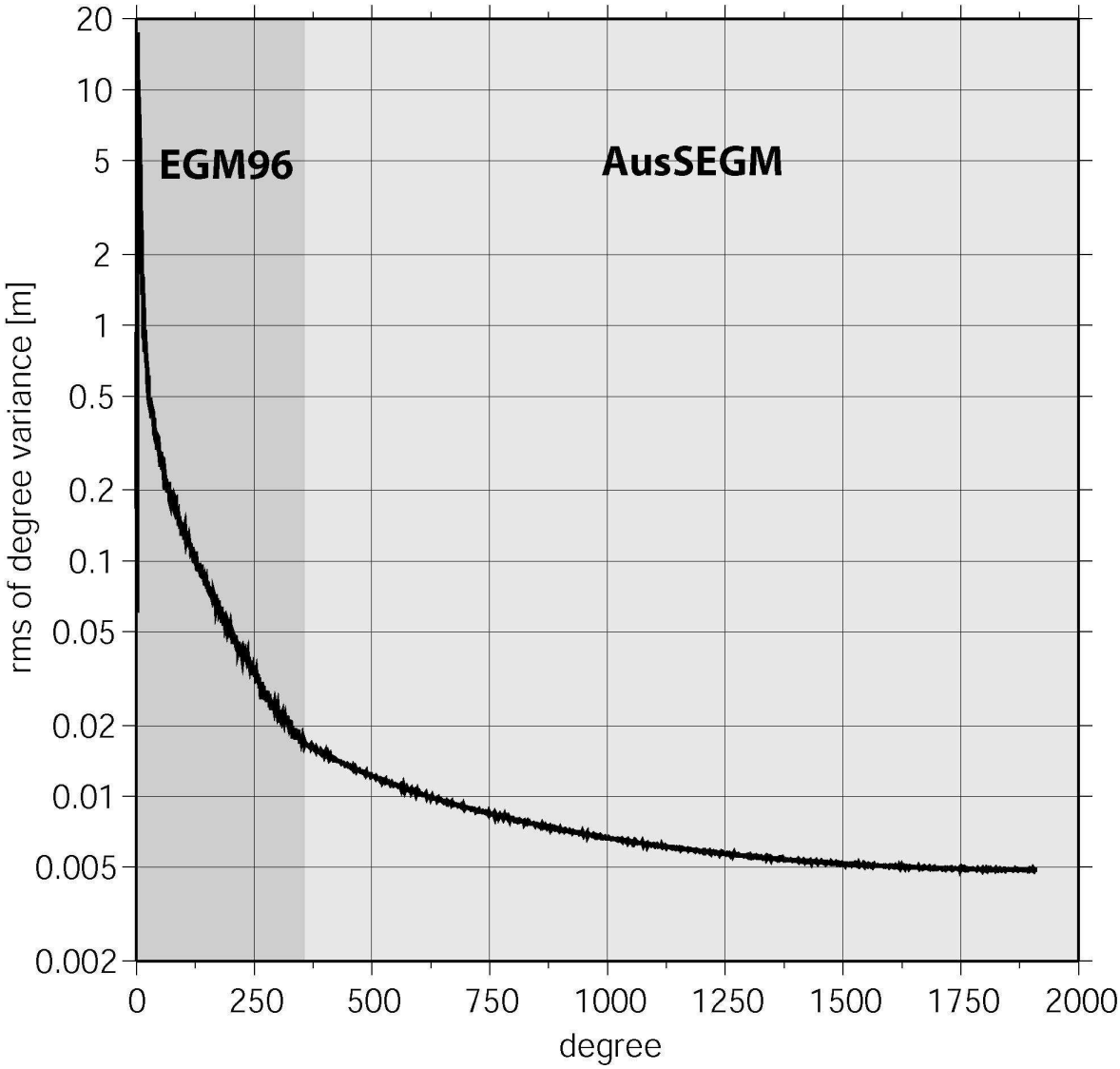

Figure 12: Degree variances (signal power) for the geoid height taken from EGM96 (up to N_{max} = 360) and the PSD of AusSEGM geoid heights (beyond N_{max} = 360).

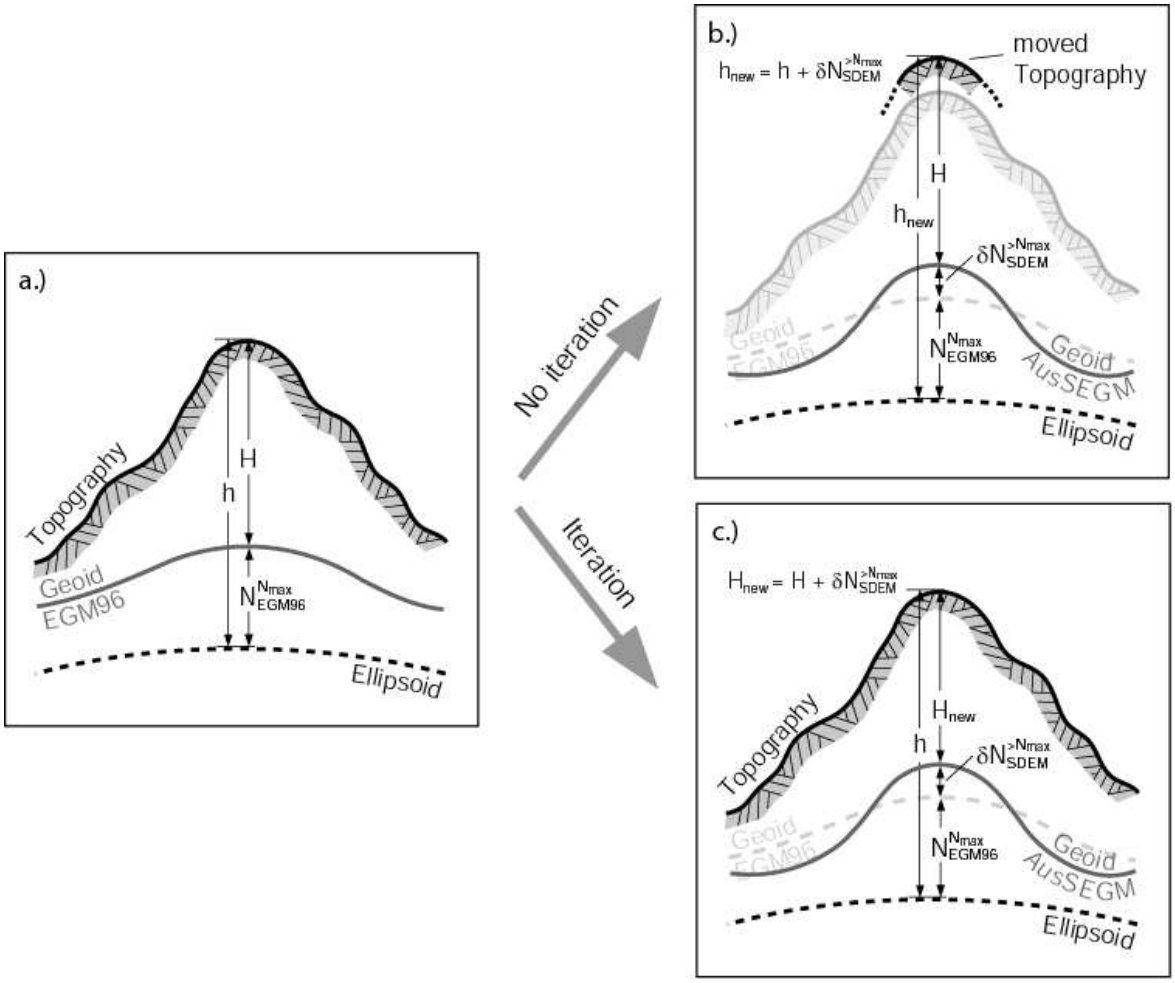

Figure 13: Schematic illustration of the iterative computation procedure. a) *Initial situation:* Heights H are referred to the geoid given by EGM96. b.) *No iteration:* Heights H are referred to the new synthetic geoid and remain unchanged. The ellipsoid height h is changed by $\delta N^{N_{max}}_{SDEM}$. c.) *Iteration:* Heights H are referred to the new synthetic geoid and are changed by $\delta N^{N_{max}}_{SDEM}$. The ellipsoid height h remains unchanged.